# Single-cell RNA sequencing reveals that *BMPR2* mutation regulates right ventricular function *via ID* genes

Mingxia Du[1,2], Haibin Jiang[1,2], Hongxian Liu[1,2], Xin Zhao[1,2], Yu Zhou[3], Fang Zhou[2], Chunmei Piao[4], Guoqiang Xu[5], Feng Ma[6], Jianan Wang[7], Frederic Perros[8], Nicholas W. Morrell[9], Hong Gu[4] and Jun Yang ⓘ[1]

[1]Dept of Physiology, and Dept of Cardiology of the Second Affiliated Hospital, Zhejiang University School of Medicine, Hangzhou, China. [2]Institute of Basic Medical Sciences, Chinese Academy of Medical Sciences and School of Basic Medicine, Peking Union Medical College, Beijing, China. [3]Dept of General Intensive Care Unit, The Second Affiliated Hospital of Zhejiang University School of Medicine, Hangzhou, China. [4]Dept of Pediatric Cardiology, Beijing Anzhen Hospital, Capital Medical University, Beijing, China. [5]Jiangsu Key Laboratory of Neuropsychiatric Diseases and College of Pharmaceutical Sciences, Jiangsu Key Laboratory of Preventive and Translational Medicine for Geriatric Diseases, Soochow University, Suzhou, China. [6]Institute of Blood Transfusion, Chinese Academy of Medical Sciences, Chengdu, China. [7]Dept of Cardiology of the Second Affiliated Hospital, Zhejiang University School of Medicine, Hangzhou, China. [8]Université Paris–Saclay, AP-HP, INSERM UMR_S 999, Service de Pneumologie et Soins Intensifs Respiratoires, Hôpital de Bicêtre, Le Kremlin Bicêtre, France. [9]Dept of Medicine, University of Cambridge School of Clinical Medicine, Addenbrooke's Hospital, Cambridge, UK.

Corresponding author: Jun Yang (yang_jun@zju.edu.cn)

## Abstract

*Background* Mutations in bone morphogenetic protein type II receptor (*BMPR2*) have been found in patients with congenital heart disease-associated pulmonary arterial hypertension (CHD-PAH). Our study aimed to clarify whether deficient BMPR2 signalling acts through downstream effectors, inhibitors of DNA-binding proteins (IDs) during heart development to contribute to the progress of PAH in CHD patients.

*Methods* To confirm that IDs are downstream effectors of BMPR2 signalling in cardiac mesoderm progenitors (CMPs) and contribute to PAH, we generated cardiomyocyte-specific *Id 1/3* knockout mice (Ids cDKO), and 12 out of 25 developed mild PAH with altered haemodynamic indices and pulmonary vascular remodelling. Moreover, we generated *ID1* and *ID3* double-knockout (IDs KO) human embryonic stem cells that recapitulated the BMPR2 signalling deficiency of CHD-PAH induced pluripotent stem cells (iPSCs).

*Results* Cardiomyocytes differentiated from iPSCs derived from CHD-PAH patients with BMP receptor mutations exhibited dysfunctional cardiac differentiation and reduced calcium ($Ca^{2+}$) transients, as evidenced by confocal microscopy experiments. Smad1/5 phosphorylation and ID1 and ID3 expression were reduced in CHD-PAH iPSCs and in *Bmpr2*^{+/−} rat right ventricles. Moreover, ultrasound revealed that 33% of Ids cDKO mice had detectable defects in their ventricular septum and pulmonary regurgitation. Cardiomyocytes isolated from mouse right ventricles also showed reduced $Ca^{2+}$ transients and shortened sarcomeres. Single-cell RNA sequencing analysis revealed impaired differentiation of CMPs and downregulated USP9X expression in IDs KO cells compared with wild-type cells.

*Conclusion* We found that BMPR2 signals through IDs and USP9X to regulate cardiac differentiation, and the loss of ID1 and ID3 expression contributes to cardiomyocyte dysfunction in CHD-PAH patients with *BMPR2* mutations.

## Introduction

Pulmonary arterial hypertension (PAH) is a progressive disease with pathological characteristics that include the thickening and narrowing of pulmonary microvessels, which leads to elevated pulmonary

vascular resistance and right ventricular hypertrophy and often results in right ventricular failure [1, 2]. In the past two decades, mutations in components of the bone morphogenetic protein (BMP) signalling pathway have been found in patients with the genetic form of PAH [3]. For example, mutations in *BMPR2* have been identified in patients with congenital heart disease-associated PAH (CHD-PAH) [4]. To date, related studies have focused on pulmonary vascular remodelling to understand the aetiology of PAH/ CHD-PAH with *BMPR2* mutations [5, 6]. Whether the final heart failure in patients with PAH is related to a primary cardiomyocyte abnormality has not been elucidated.

Although a previous study provided evidence that cardiac defects, including ventricular septal defects (VSD), might be caused by embryonic *BMPR2* mutations in mice, whether the mice had PAH was not reported because of the short lifespan associated with this mutation [7]. Moreover, a recent study demonstrated that rats with a monoallelic mutation in *Bmpr2* spontaneously developed PAH after 6 months and that their right ventricular cardiomyocytes exhibited reduced calcium ($Ca^{2+}$) responsiveness compared with those from wild-type rats [8]. Cardiac output was even reduced in nonspontaneous PAH rats, and a further study suggested that the right ventricular cardiomyocytes of *Bmpr2* mutant rats lacked the adaptation of cardiomyocytes from wild-type rats. Before this report, evidence was available only for heart defects from subjects with CHD-PAH to support our hypothesis that mutated *BMPR2* affects the cardiomyocytes in patients with PAH.

Inhibitors of DNA-binding proteins (IDs) are helix-loop-helix (HLH) transcription factors and have been reported to be important target downstream of BMP receptors during cardiogenesis [9, 10]. In our previous review, we speculated that BMPR2 contributes to cardiac formation during development *via* the downstream effector gene *Id* based on the similar phenotypes of *Id* knockout (KO) mice and BMPR2 mox-cre KO mice [11]. A recent study showed that *Id* genes are critical for cardiac development since quadruple KO of four subtypes of *Ids* (1–4) in mice led to the absence of cardiac development [12]. BMP receptors convey signalling through phosphorylated Smad1/5 to induce IDs expression in most cell types, and the mutations of *BMPR2* and *BMP type I receptors* reported in PAH/CHD-PAH may affect IDs and thereby affect cardiomyocyte gene transcription.

In the present study, we aimed to clarify that ID1 and ID3 are important for PAH development and are responsible for the effect of mutant *BMPR2* on cardiomyocytes. We found that cardiomyocyte *Id 1/3* KO mice developed PAH. Moreover, single-cell (sc)RNA sequencing (seq) analysis provided novel evidence of human embryonic stem cells (hESCs) lacking *ID1/3* genes differentiated less towards cardiomyocytes and of the BMPR2 downstream effectors ID1/3 coordinately regulating heart development through USP9X. Cardiomyocyte *Id 1/3* KO mice developed PAH, which further strengthens the knowledge of the impact of BMPR2 signalling on heart development and the onset of PAH/CHD-PAH. The poor prognosis of these patients necessitates genetic screening for suspicious genes, including *BMPR2* and other signalling pathway components.

## Methods
All supporting data and methods are available within the article and the online supplementary material; the expanded materials and methods section is available in the online supplementary material.

### Establishment of patient-specific induced pluripotent stem cell lines
Somatic reprogramming was used to generate induced pluripotent stem cell (iPSC) lines from peripheral blood mononuclear cells (PBMCs) harvested from four patients with CHD-PAH and four healthy subjects using the Sendai virus reprogramming protocol, as described previously [13]. More detailed descriptions are provided in the supplementary material and table S1.

### Establishment of ID1 *and* ID3 *double-knockout cell lines*
The *ID1* and *ID3* CRISPR/Cas9 plasmids were generated according to a previous report [14]. These two plasmids were transfected into H9 cells, and clones were selected with puromycin. A detailed description is provided in the supplementary material.

### Ethical considerations
Written informed consent was provided by all participants prior to the start of the study. This study was approved by the institutional review board of the Institute of Basic Medical Sciences, Chinese Academy of Medical Sciences, Beijing (014–2015) and Zhejiang University (2021-020), China.
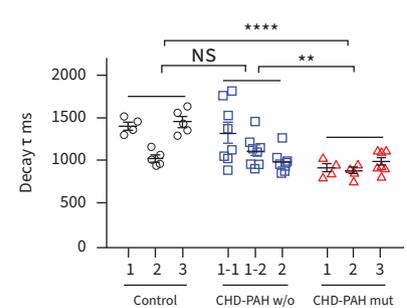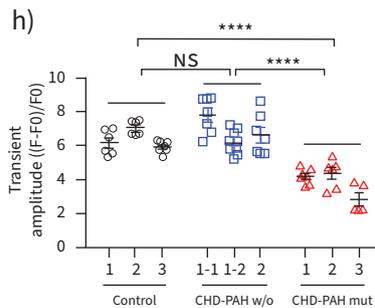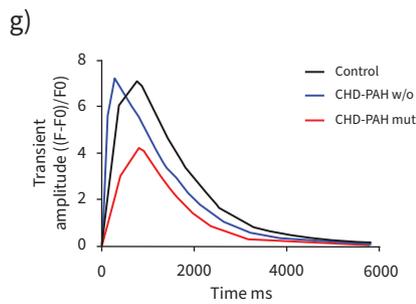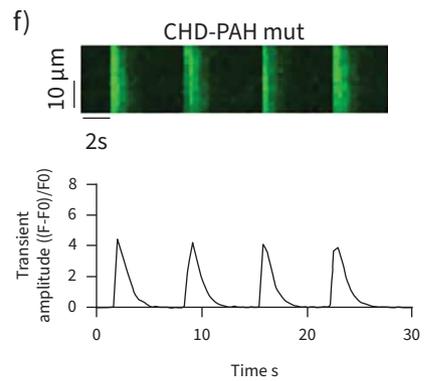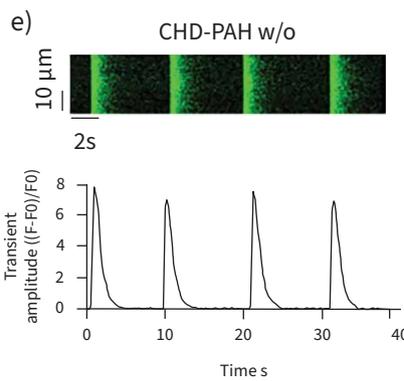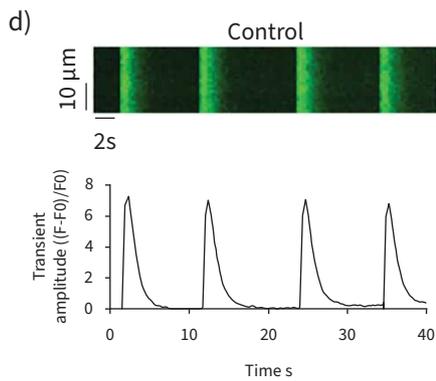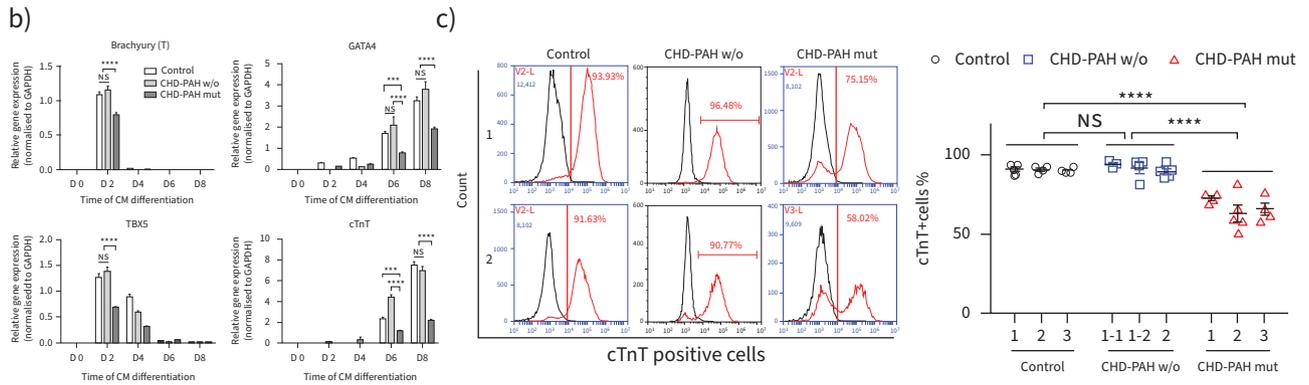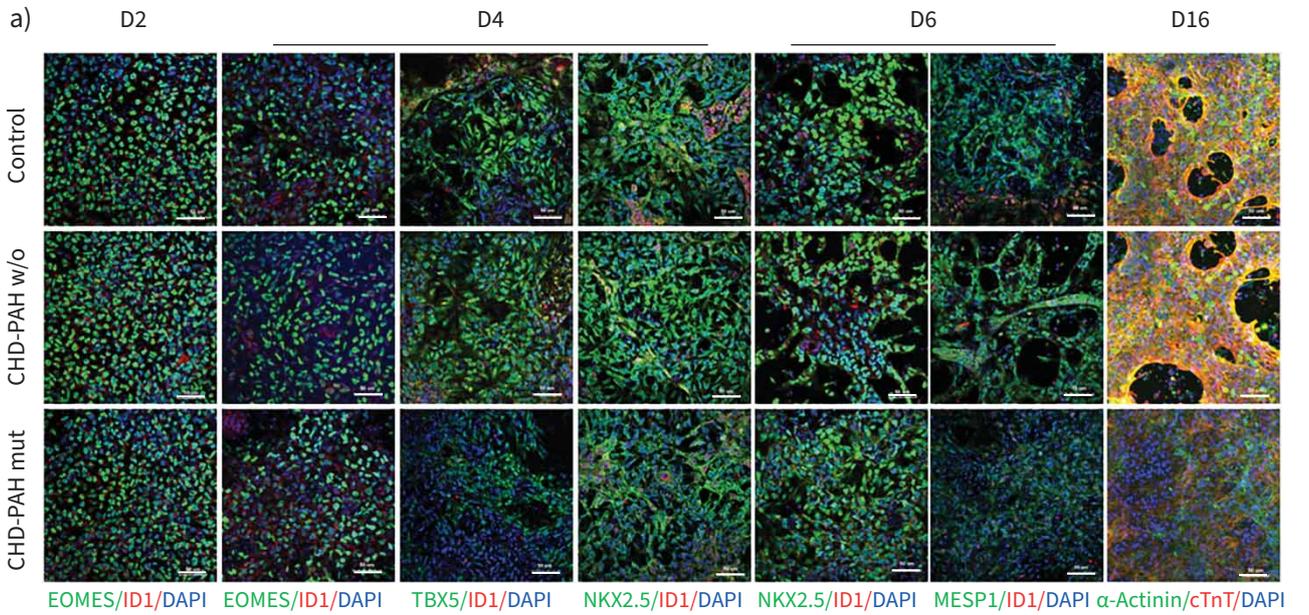
FIGURE 1 Bone morphogenetic protein type II receptor (*BMPR2*) mutation impairs the differentiation and calcium ($Ca^{2+}$) transients of cardiomyocytes (CMs) derived from congenital heart disease-associated pulmonary arterial hypertension (CHD-PAH) induced pluripotent stem cells (iPSCs). a) Immunofluorescence of EOMES, TBX5, NKX2.5, MESP1, α-Actinin, cTnT and inhibitor of DNA-binding proteins (ID)1 as determined using 4′,6-diamidino-2-phenylindole (DAPI) as a counterstain on days 2, 4, 6 and 16 of CM differentiation. Scale bars=50 μm. b) mRNA levels of *Brachyury* (*T*), *GATA4*, *TBX5* and *cTnT* were measured using quantitative PCR during CM differentiation from iPSCs, n=3. c) Fluorescence-activated cell sorting analyses (left) and quantification (right) of the percentages of cTnT$^+$ cells on day 16 of CM differentiation from three control, three CHD-PAH without *BMPR* mutation (w/o) and three CHD-PAH with *BMPR* mutation (mut) iPS cell lines; 4–6 repeats for each cell line. Cell line 1–1 and 1–2 in CHD-PAH w/o group were obtained from the same patient. n=12–14. d–f) Representative $Ca^{2+}$ imaging as determined by recording Fluo-4/AM traces in d) control iPSC-derived CMs, e) CHD-PAH w/o iPSC-derived CMs and f) CHD-PAH mut iPSC-derived CMs. g) Comparison of $Ca^{2+}$ transients of control, CHD-PAH w/o and CHD-PAH mut CMs in a single beating episode. h) Statistical analysis of $Ca^{2+}$ handling features, such as the amplitude of $Ca^{2+}$ transients (left) and τ decay (right); 5–8 cells for each iPSC-CM line; n=18–24. All results are presented as mean±SEM. **: p<0.01, ***: p<0.001, ****: p<0.0001 *versus* control, CHD-PAH w/o or CHD-PAH mut group as determined using two-way ANOVA with *post hoc* tests (Tukey's multiple comparisons test) (b, c and h).

### Statistical analysis

The t-test, one-way ANOVA and two-way ANOVA were used for statistical analyses, which were performed using GraphPad Prism 6.0. All data are presented as mean±SEM.

### Results

#### *BMPR2 mutation impairs the differentiation of CHD-PAH iPSCs towards cardiomyocytes and reduces the cardiomyocyte $Ca^{2+}$ transients*

To examine the effects of *BMPR2* mutation on cardiomyocytes in the context of CHD-PAH, we generated iPSCs from CHD-PAH patients with BMP receptor (*BMPR*) mutations (CHD-PAH mut iPSCs), without *BMPR* mutation (CHD-PAH w/o iPSCs) and healthy donors (control iPSCs) by reprogramming the PBMCs with the Sendai virus and characterised the mutations according to the clinical phenotypes of the CHD-PAH patients, including three mutation carriers with mild secundum atrial septal defects (ASDs) and one mutation carrier with a patent ductus arteriosus (PDA) defect (supplementary figure S1a and supplementary tables S1 and S9). All cell lines exhibited human pluripotent stem cell-like morphologies with flat and compact cell clones and pluripotency marker gene expression (supplementary figure S1b).

Control and CHD-PAH iPSCs (with/without *BMPR2* mutation) were then differentiated into cardiomyocytes that spontaneously contracted rhythmically. Immunofluorescence staining showed decreased expression of EOMES on day 2 and the cardiogenic specific TBX5 and NKX2.5 on day 4 (figure 1a). The effects on NKX2.5 and MESP1 were more obvious in differentiated CHD-PAH mut cells on day 6 (figure 1a and supplementary figure S2a). Both control and CHD-PAH iPSC-differentiated cells expressed the cardiomyocyte-specific markers cTnT and α-Actinin on day 16 after differentiation (figure 1a), but CHD-PAH mut cells had little expression of cTnT. A real-time PCR assay showed that the expression of *Brachyury* (*T*) and *TBX5* was significantly reduced in mutant CHD-PAH cells compared with control and CHD-PAH w/o cells on day 2. *GATA4* and *cTnT* expression were significantly decreased in mutant cells on day 6 and day 8 (figure 1b). On day 16 of differentiation, fluorescence-activated cell sorting analysis showed that 90.84±0.26% and 91.80±1.36% of the cells differentiated from control and CHD-PAH w/o iPSCs expressed cTnT, while significantly fewer cells differentiated from CHD-PAH iPSCs expressed cTnT (67.32±2.91%, p<0.001) (figure 1c). Thus, iPSCs from CHD-PAH patients with *BMPR2* mutations differentiated into mature cardiomyocytes that differed from the cardiomyocytes differentiated from control and CHD-PAH w/o iPSCs.

To determine the functional characteristics of the differentiated cardiomyocytes, we examined the spontaneous $Ca^{2+}$ transients in three lines of mature control cardiomyocytes, three lines of CHD-PAH w/o cardiomyocytes and three lines of CHD-PAH mut cardiomyocytes *via* upright confocal microscopy. Both the control and CHD-PAH cardiomyocytes maintained rhythmicity based on the detection of store-operated $Ca^{2+}$ entry (figure 1d–f and supplementary figure S2b). Notably, the $Ca^{2+}$ transient amplitude, decay τ and half decay time of cardiomyocytes derived from CHD-PAH mut iPSCs were significantly reduced compared with those derived from the control and CHD-PAH w/o iPSCs (figure 1g,h and supplementary figure S2c); however, there were no significant differences in the half rising time or the time to peak (supplementary figure S2c), indicating that the $Ca^{2+}$ storage in CHD-PAH mut cardiomyocytes was impaired *via* either sarcoplasmic reticulum dysfunction or the efflux of $Ca^{2+}$ through the sodium ($Na^+$)–$Ca^{2+}$ exchanger. Additionally, the regularities of the control and CHD-PAH mut cardiomyocytes regarding the sarcomeric protein arrangement were similar when the signals *via* fast Fourier transformation were analysed, and there was no difference in the correlation coefficients based on the costaining of α-Actinin
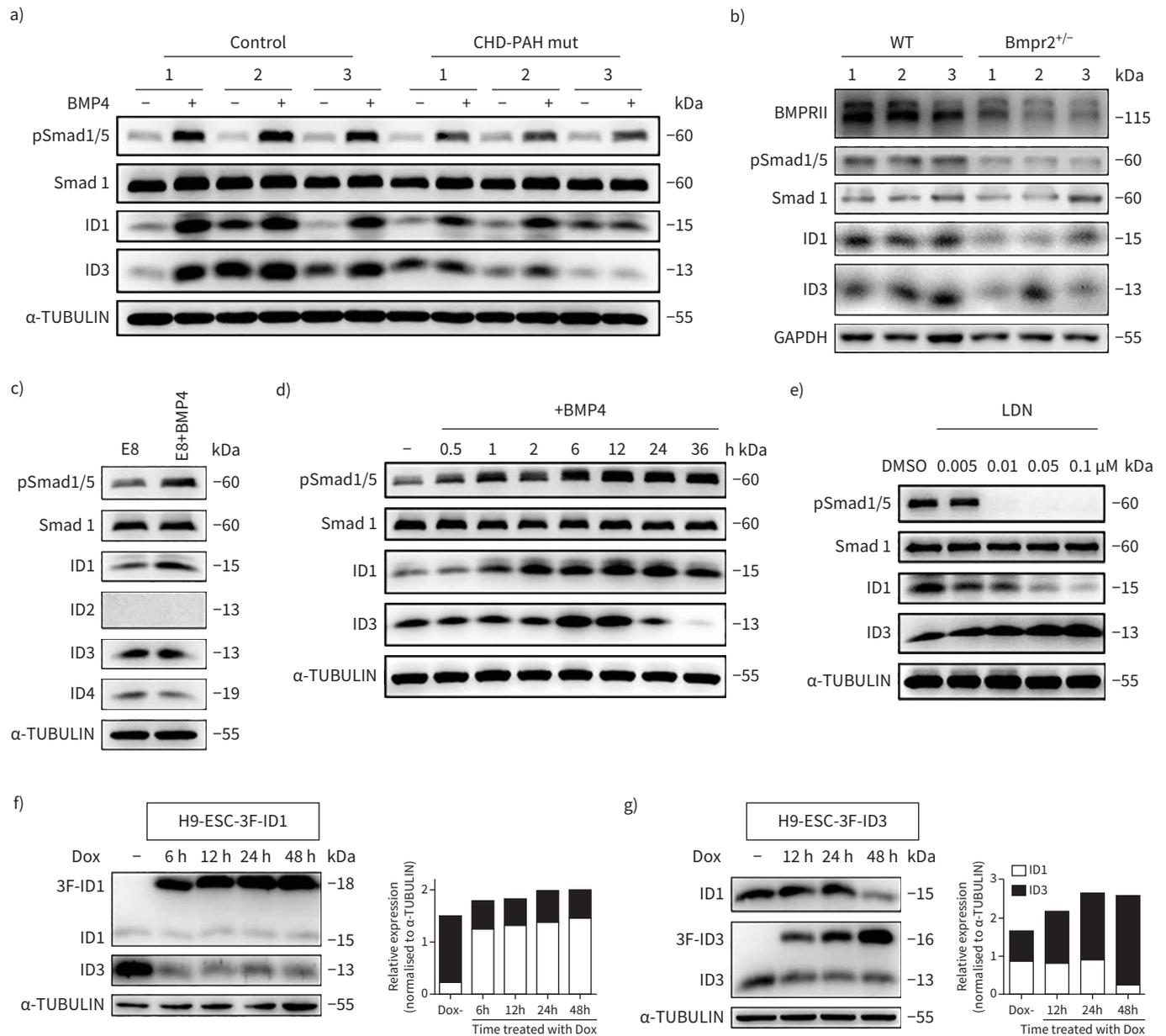
FIGURE 2 Reduced inhibitors of DNA-binding proteins (ID)1/ID3 expression in congenital heart disease-associated pulmonary arterial hypertension (CHD-PAH) induced pluripotent stem cells (iPSCs) with bone morphogenetic protein type II receptor (*BMPR2*) mutations (mut) and the coordinative regulation between ID1 and ID3. a) Representative immunoblot analysis of the pSmad1/5, ID1 and ID3 levels in CHD-PAH mut and control iPSCs treated with or without 30 ng·mL$^{-1}$ BMP4 for 2 h. α-TUBULIN was used as loading control. b) Representative immunoblotting of BMPRII, pSmad1/5, ID1 and ID3 in the right ventricles of wild-type (WT) and *Bmpr2*$^{+/-}$ rats. The results from three rats (marked as 1/2/3) are presented simultaneously. GAPDH was used as the loading control. c) Immunoblot analysis of human embryonic stem cells (hESCs) cultured with or without 30 ng·mL$^{-1}$ BMP4 for 2 h. α-TUBULIN was used as the loading control. d) Immunoblot time-course analysis of pSmad1/5, Samd1, ID1 and ID3 expression in hESCs stimulated without (0 h) and with 30 ng·mL$^{-1}$ BMP4 for 0.5–36 h. Smad1 and α-TUBULIN were used as loading controls. e) Immunoblot analysis of the ID1 and ID3 levels in hESCs stimulated with DMSO or LDN193189 (LDN) at different concentrations for 24 h. Smad1 and α-TUBULIN were used as loading controls. f) Immunoblot and densitometric analyses of total ID1 (endogenous (lower band) and exogenous (upper band)) and ID3 expression in the 3xFlag-ID1 inducible overexpression line h9-ESC-3F-ID1 treated with Dox (2 µg·mL$^{-1}$). α-TUBULIN was used as the loading control. g) Immunoblot and relative densitometric analyses of total ID3 (endogenous (lower band) and exogenous (upper band)) and ID1 expression in the 3xFlag-ID3 inducible overexpression line h9-ESC-3F-ID3. α-TUBULIN was used as the loading control. All cells were cultured in E8 medium (a and c–g). E8: Essential 8 Medium (composition shown in supplementary table S8); Dox: doxycycline.

and cTnT (supplementary figure S2d,e). These results suggested that *BMPR2* mutation impacted the differentiation and Ca$^{2+}$ handling of CHD-PAH iPSC-cardiomyocytes.

### ID1 and ID3 expression levels are reduced in CHD-PAH iPSCs with *BMPR2* mutation, and exhibit coordinated regulation

BMP4 is important for cardiovascular developmental processes, including heart formation and vasculogenesis [15, 16]. Thus, we stimulated control and CHD-PAH iPSCs with BMP4 to examine their responsiveness to BMPR2 signalling based on the phosphorylation of Smad1/5 and the expression of ID1 and ID3, which are major downstream effector genes of BMPR2 signalling in both humans and mice [17, 18]. After treatment with 30 ng·mL$^{-1}$ BMP4 for 2 h, immunoblotting showed that the ID1 levels were lower in the CHD-PAH mut iPSC lines than in the control iPSC lines (figure 2a and supplementary figure S3a). Similar results were found in the *BMPR1b*-mutated CHD-PAH line (supplementary figure S3b). CHD-PAH w/o iPSCs had intact pSmad1/5 and ID1 level (supplementary figure S3c). These results showed reduced BMPR2/ID signalling in CHD-PAH iPSCs with *BMPR* mutations.

In addition, we evaluated the effects of the monoallelic deletion of *Bmpr2* (*Bmpr2$^{+/-}$*) on BMPRII protein expression and downstream signalling pathways in the right ventricles of rats. As expected, the protein expression of BMPRII was reduced by 50% in the right ventricular tissues of 6-month-old *Bmpr2* mutant rats (*Bmpr2$^{+/-}$*). We observed significant decreases in the protein levels of pSmad1/5 and Id1/Id3 in the right ventricles of *Bmpr2$^{+/-}$* rats compared with those of wild-type rats (figure 2b and supplementary figure S3d). This result suggests that the monoallelic deletion of *Bmpr2* also decreases the Id1 and Id3 protein expression levels *in vivo*.

We then studied the relationships between the BMPR2 signalling pathway and ID proteins in hESCs (the h9 cell line), which have the same differentiation potential and mutation generation characteristics as iPSCs, for gene function analysis. Immunoblotting showed that the protein levels of IDs (ID1, ID2, ID3 and ID4) were similar in the two conventional culture conditions. Specifically, the ID1 and ID3 proteins were more abundant than ID4, and no detectable expression of ID2 was observed (supplementary figure S3e). We examined the baseline ID1 expression with a luciferase/ID1-GFP reporter line (supplementary figure S3f) and found that the *ID1* promoter activity was significantly increased by BMP9, which was reported to activate *BMPR2* (supplementary figure S3g). Immunoblotting analysis demonstrated that ID1 was induced, while ID3 expression was less affected by BMP4 treatment for 2 h (figure 2c). We also showed the time course of ID1/3 induction by BMP4 stimulation for 36 h, and found the induction of ID3 reached maximum level at 6–12 h after BMP4 stimulation; thereafter ID1 was the major form downstream of BMPR2 signalling (figure 2d).

To further investigate the regulation of ID1 and ID3 by BMP receptor, hESCs were treated with LDN193189 (LDN), a known inhibitor of activin receptor-like kinase (ALK)2. The expression of ID1 was decreased as reported [19], while the protein expression of ID3 was simultaneously increased in the absence of BMP4 (figure 2e). We established the ID1- and ID3-inducible overexpression cell lines H9-ESC-3F-ID1 and H9-ESC-3F-ID3, respectively, with a lentivirus tet-on 3G inducible expression system (supplementary figure S3h and i). Decreased ID3 expression was observed when ID1 overexpression was induced with doxycycline (Dox) (figure 2f). In contrast, reduced ID1 protein levels were observed when ID3 was overexpressed (figure 2g). Taken together, our results suggested that the expression of ID1/ID3 was reduced in CHD-PAH iPSCs with *BMPR2* mutations and that ID1 and ID3 exhibited coordinated regulation.

### Ids conditional double-knockout mice are susceptible to PAH and pulmonary vascular remodelling

To investigate the roles of *Id* genes in the intrinsic alterations of the heart in PAH and bypass the limitation of the embryonic lethality of *Id1* and *Id3* double knockout [10], we crossed *Id1* knockout (KO) mice (Id1$^{-/-}$) with mice harbouring a flox insertion in the *Id3* allele (Id3$^{f/w}$) and targeted *Id3* ablation in the pre-cardiac mesoderm by utilising CRE recombinase, which was driven by the earliest cardiovascular progenitor marker Mesp1 (Mesp1-cre mice), thereby generating *Ids* conditional double-knockout mice (Ids cDKO) (supplementary figure S4a). After genotyping, we confirmed that the decreased protein expression of Id1 and Id3 in mouse hearts (E18.5) was consistent with the PCR results (supplementary figure S4b). Then, we performed ultrasonic scanning on 2-month-old mice (adult). Significant decreases in the right ventricular cardiac output and tricuspid annular plane systolic excursion (TAPSE) were detected in Id1$^{-/-}$Id3$^{f/w}$;Mesp1-cre and Id1$^{+/-}$Id3$^{f/f}$;Mesp1-cre mice compared to control mice (supplementary figure S4c). There were no significant differences in the left ventricular ejection fraction (LVEF) or left ventricular fractional shortening (LVFS) among the control, Id1$^{-/-}$Id3$^{f/w}$;Mesp1-cre and Id1$^{+/-}$Id3$^{f/f}$; Mesp1-cre mice (supplementary figure S4d), indicating that the Ids cDKO mice could develop PAH.

Next, cardiac catheterisation was performed on 6-month-old mice to compare the haemodynamic indices of the two types of Ids cDKO mice and control mice. A substantial proportion of mice (five out of 12 Id1$^{-/-}$Id3$^{f/w}$;Mesp1-cre and seven out of 13 Id1$^{+/-}$Id3$^{f/f}$;Mesp1-cre mice) developed significantly elevated
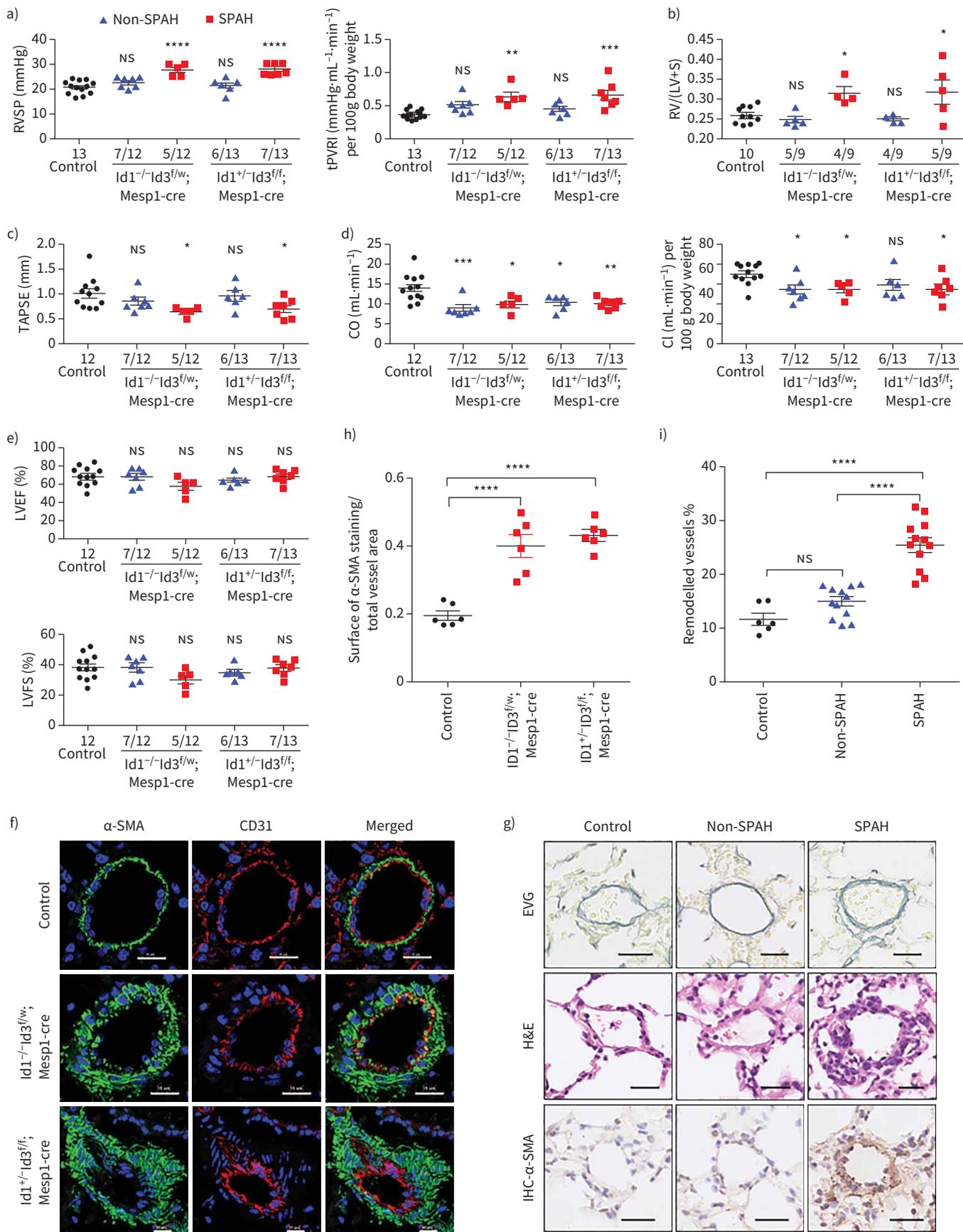
**FIGURE 3** *Id 1/3* knockout mice (Ids cDKO) mice are susceptible to pulmonary arterial hypertension (PAH) and pulmonary vascular remodelling. a–e) Assessment of a) right ventricular systolic pressure (RVSP) and total pulmonary vascular resistance index (tPVRI) (tPVRI=RVSP/cardiac index); b) Fulton index (right ventricular hypertrophy, RV/(LV+S)); c) tricuspid annular plane systolic excursion (TAPSE); d) cardiac output (CO) and cardiac index (CI) (cardiac output/body weight); and e) left ventricular ejection fraction (LVEF) and left ventricular fraction shortening (LVFS) in control mice (control) and Id cDKO mice without spontaneous arterial hypertension (non-SPAH) or with SPAH at age 6 months. Mice were defined as having SPAH when their RVSP was >25 mmHg. The numbers of mice that did or did not develop SPAH among the total mice in each group are shown on the x-axis. f) Representative immunofluorescence staining of α-actin smooth muscle (α-SMA, green) and the endothelial cell marker CD31 (red) in lung sections revealed thickened arterial walls in Id cDKO mice with SPAH at 6 months of age. Nuclei were counterstained with 4′,6-diamidino-2-phenylindole (blue). Scale bars=15 μm. g) Representative images of vascular remodelling in the distal arterioles stained with elastin and immunostained (IHC) α-SMA, and representative images of pulmonary arteries stained with haematoxylin and eosin (H&E). The lung sections were obtained from control and Id cDKO mice with non-SPAH or SPAH at 6 months of age. Scale bars–25 μm. h) Vessel muscularisation analysis based on α-SMA labelling on the lung sections from control and Id cDKO mice with SPAH at 6 months of age. i) Pulmonary vascular remodelling rate based on Elastica van Gieson (EVG) staining on the lung sections from control and Id cDKO mice with or without SPAH at 6 months of age. The vessels 25–100 μm in diameter in f) and g) were quantified and n=6–12 mice for each group in h) and i). RV: right ventricle; LV: left ventricle; S: septum; NS: nonsignificant. All results are presented as mean±SEM. *: $p<0.05$, **: $p<0.01$, ***: $p<0.001$ and ****: $p<0.0001$ *versus* control and other groups as determined using one-way ANOVA with *post hoc* tests (Dunnett's multiple comparisons test in panels a–e and h, and Tukey's multiple comparisons test in panel i.

right ventricular systolic pressure (RVSP) and total pulmonary vascular (PVR) resistance, referred to as spontaneous PAH (SPAH), while the other Ids cDKO mice did not develop PAH (non-SPAH) (figure 3a and supplementary figure S4e). The mice with SPAH showed worse right ventricular function, with a higher Fulton index and lower TAPSE, cardiac output and cardiac index values than the control mice (figure 3b–d). Although the RVSP was not elevated in non-SPAH mice, the reduced cardiac output and cardiac index values suggested that heart function was also affected in these mice (figure 3d). Notably, however, the unchanged LVEF and LVFS in all Ids cDKO mice indicated that left heart function was not affected (figure 3e).

Immunohistochemistry of mouse lung samples with α-smooth muscle actin (SMA) and CD31 staining revealed the increased muscularisation of pulmonary microvessels in SPAH mice (with diameters 100 μM) (figure 3f and 3h). Elastin Van Gieson staining demonstrating the significantly thickened pulmonary arterial wall in SPAH mice, but not in non-SPAH mice compared with control mice, which suggested that pulmonary vascular remodelling occurred in SPAH mice (figure 3g and 3i). These results suggested that the Ids cDKO mice were susceptible to pulmonary vascular remodelling.

### Ventricular defects and reduced Ca²⁺ transients in cardiomyocytes compromise right heart function in Ids cDKO mice

To assess the heart defects of Ids cDKO mice, we employed colour Doppler echocardiography. We observed abnormal blood flow in the hearts of 33.3% of the Ids cDKO mice at 2 months, including reflux of the tricuspid valve (one mouse), VSDs (two mice) and pulmonary valve defects (six mice) (figure 4a). 50% of the mice with reflux had PAH at 6 months. Pulmonary valve regurgitation was detected during diastole in Ids cDKO mice, but not in control mice (figure 4b). Additionally, VSDs were clearly identified by ultrasonic scanning and in sequentially sliced heart sections (figure 4c and 4d). The cardiomyocytes of the middle and outer myocardial wall of the right ventricle from Ids cDKO mice were smaller than those from control mice (figure 4e and 4f). Such differences were not found in cardiomyocytes of the interventricular septum.

To examine the function of cardiomyocytes, we isolated cardiomyocytes from control and Ids cDKO mice. Significantly reduced Ca²⁺ transients and sarcomere length shortening were found in cardiomyocytes isolated from the right ventricles of Ids cDKO mice but not in those isolated from the left ventricle compared to the control mice (figure 4g and figure 4h). Additionally, the regularities of the control and Ids cDKO cardiomyocytes were similar in regards to the sarcomeric protein arrangement when the signals *via* fast Fourier transformation were analysed, and no differences were observed in the correlation coefficients determined based on the costaining of α-Actinin and cTnT (supplementary figure S5a and b). Taken together, these results indicated that the loss of Id1 and Id3 protein expression in the heart impaired right ventricular function.

### Cardiomyocyte differentiation is impaired in ID1/ID3 double-knockout hESC lines

To clarify the effects of *BMPR2/ID* deficiency on CHD-PAH development, we generated *ID1* and *ID3* double-knockout hESC lines (IDs KO) with an episomal CRISPR/Cas9 plasmid. We designed three small guide (sg)RNAs targeting *ID1* and *ID3* (supplementary table S5) and then transfected vectors into 293T cells to identify the sgRNA with the highest editing efficiency (supplementary figure S6a–c). We successfully subcloned three *ID1* and *ID3* double-knockout lines (IDs KOs), two *ID1⁻/⁻* lines, three *ID3⁻/⁻* lines and two *ID3⁻/⁻ID1⁻/⁺* lines (figure 5a, supplementary figure S6d and e). Next, we differentiated these
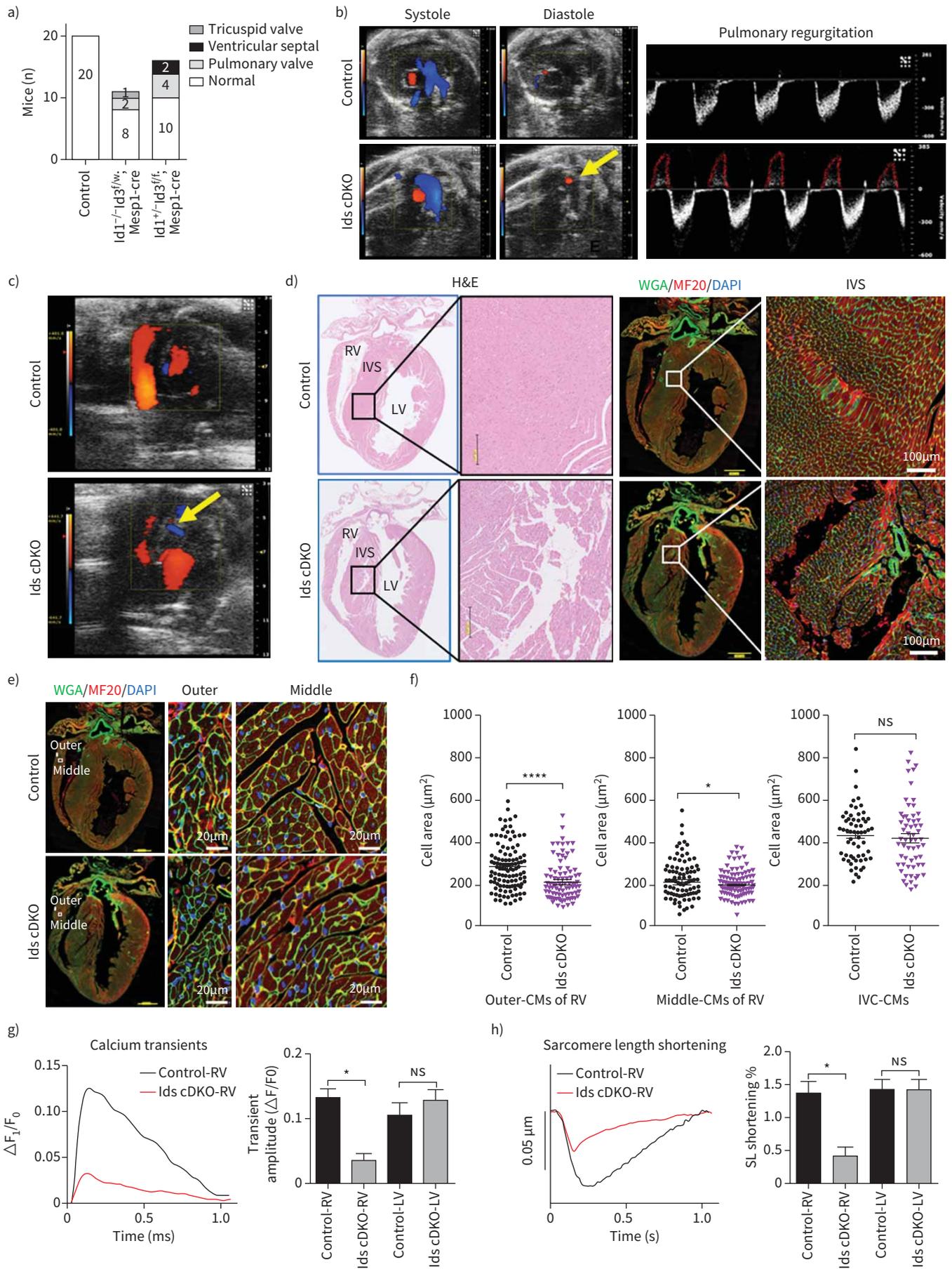
**FIGURE 4** Ventricular defects and reduced calcium ($Ca^{2+}$) transients in cardiomyocytes (CMs) compromised the right heart function in *Id 1/3* knockout mice (Ids cDKO) mice. a) Types of blood reflux in the hearts of 2-month-old wild-type (control) (n=20), $Id1^{-/-}Id3^{f/w}$;Mesp1-cre (n=11) and $Id1^{+/-}Id3^{f/f}$;Mesp1-cre (n=16) mice as detected by colour Doppler echocardiography. b) Representative echocardiographic images (yellow arrow) and analysis of Ids cDKO and control mice, revealing regurgitation across the pulmonary valve during diastole in Id cDKO mice. c) Representative images of interventricular septum (IVS) defects (yellow arrow) in Ids cDKO mice based on colour Doppler echocardiography. d) Haematoxylin and eosin (H&E) and immunofluorescence staining of the CM markers wheat germ agglutinin (WGA) and MF20 (myosin heavy chain 1, MYH1) in longitudinal heart sections from 6-month-old mice. Scale bars=200 µm (black), 1000 µm (yellow) and 100 µm (white). e) Immunofluorescence staining of WGA and MF20 and f) quantification of the CM areas in the hearts of control and Ids cDKO mice, revealing decreased CM areas in the middle and outer myocardial walls of the right ventricles (RVs) from 6-month-old Ids cDKO mice. Scale bars=1000 µm (yellow) and 20 µm (white); n⩾60 cells. g) Representative $Ca^{2+}$ transient trace showing a decreased transient amplitude for the RV CMs of Ids cDKO mice, but no significant differences in the LV CMs. h) Representative raw traces of the sarcomere length showing decreased sarcomere length shortening in RV-CMs of Ids cDKO mice. The percentages of sarcomere length shortening were quantified in the CMs. n⩾6 cells from each heart, two mice from each group. LV: left ventricle. Data are presented as mean±SEM. *: p<0.05 and ****: p<0.0001, as determined using unpaired t-tests.
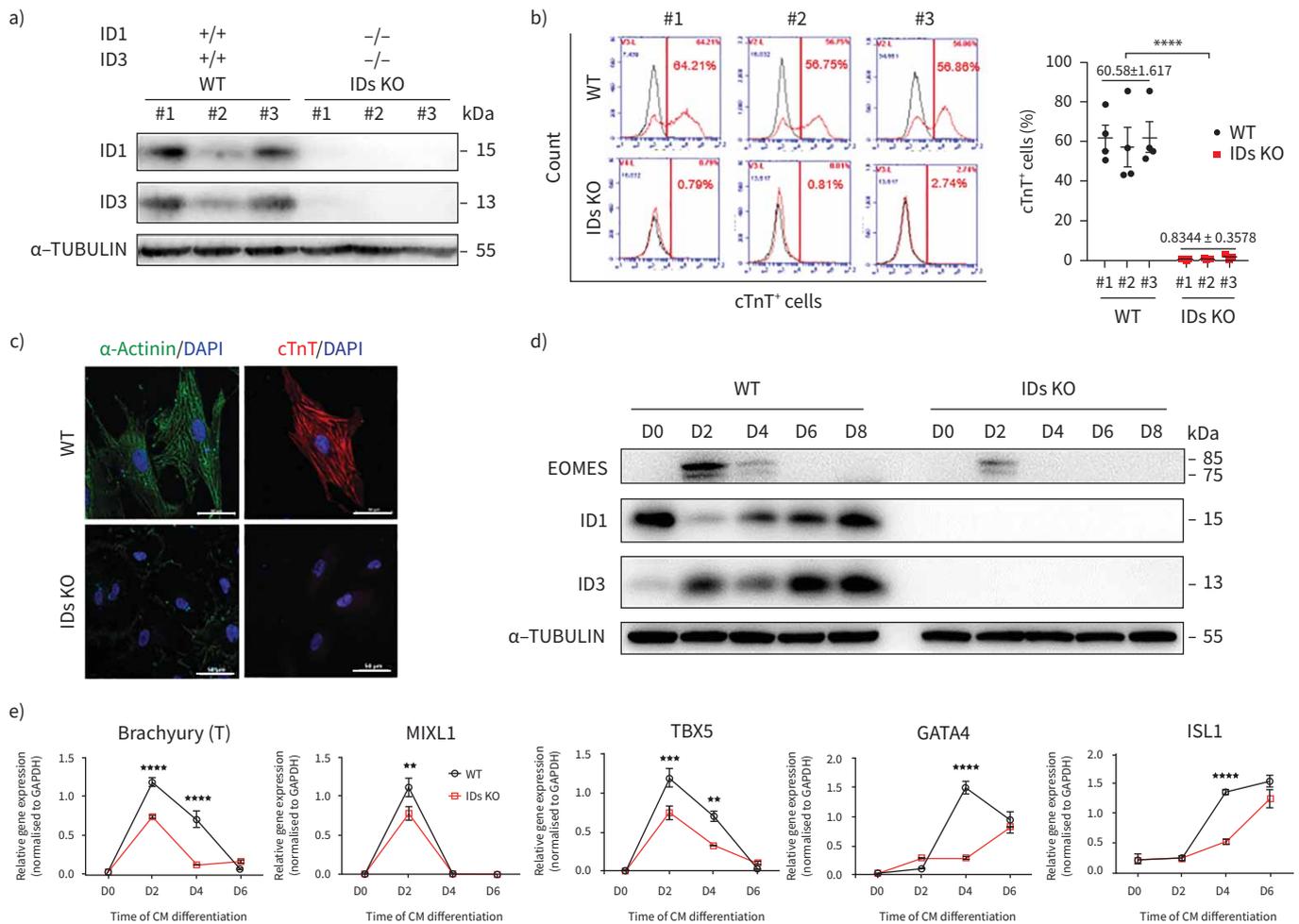


**FIGURE 5** Impaired cardiac differentiation in inhibitors of DNA-binding proteins (ID) double-knockout (KO) human embryonic stem cell (hESC) lines. a) Immunoblotting analysis of ID1 and ID3 in three IDs KO hESC lines (ID KO-#1/#2/#3) and three wild-type (WT-#1/#2/#3) cell lines. α-TUBULIN was used as a loading control. The experiment was performed three times for each cell line; n=3. b) Fluorescence-activated cell sorting (FACS) analyses (left) and quantification (right) of the percentages of cTnT+ cells on day 16 of cardiomyocyte (CM) differentiation. n=3, three repeats for each cell line; n=3, three cell lines in each group. c) Immunostaining of α-Actinin (green) and cTnT (red) in cells differentiated from WT-#1 and ID KO-#1 cell lines. 4′,6-diamidino-2-phenylindole (DAPI) was used as a counterstain and is shown in blue. Scale bars=50 µm. d) Immunoblotting of EOMES/ID1/ID3 and α-TUBULIN (as a loading control) at different stages of CM differentiation in WT and IDs KO cell lines. e) The mRNA levels of *Brachyury* (T), *MIXL1*, *TBX5*, *GATA4* and *ISL1* during CM differentiation were measured by quantitative PCR. n=3, three technical replicates for one cell line. All results are presented as mean±SEM. **: p<0.01, ***: p<0.001, ****: p<0.0001 *versus* WT and IDs KO as determined using b) unpaired t-tests and e) two-way ANOVA with *post hoc* tests (Sidak's multiple comparisons test).

| GO term (cluster 0) | p-value | GO term (cluster 3) | p-value |
|---|---|---|---|
| Negative regulation of cell migration | $7.37 \times 10^{-4}$ | Cell division | $9.68 \times 10^{-19}$ |
| Positive regulation of neuron projection | 0.006595 | Mitotic spindle organisation | $5.25 \times 10^{-6}$ |
| Nervous system development | 0.007759 | Homologous chromosome segregation | $1.55 \times 10^{-4}$ |
| Neuron migration | 0.010369 | Mitotic cell cycle phase transition | $2.58 \times 10^{-4}$ |
| Negative regulation of membrane potential | 0.012809 | Cell proliferation | 0.006552 |
| Neurotransmitter uptake | 0.033799 | G2/M transition of mitotic cell cycle | 0.008402 |
| GO term (cluster 1) | p-value | GO term (cluster 4) | p-value |
| Positive regulation of cell–cell adhesion | $4.16 \times 10^{-4}$ | Cellular response to cadmium ion | $1.88 \times 10^{-6}$ |
| Haematopoietic progenitor cell differentiation | $6.40 \times 10^{-4}$ | Cellular response to zinc ion | $3.45 \times 10^{-6}$ |
| Skeletal muscle cell differentiation | 0.006979 | Somatic stem cell population maintenance | 0.009934 |
| Positive regulation of fibroblast apoptosis | 0.015269 | G1/S transition of mitotic cell cycle | 0.010417 |
| Osteoblast differentiation | 0.029094 | Cell proliferation | 0.020916 |
| GO term (cluster 2) | p-value | GO term (cluster 5) | p-value |
| Cardiac right ventricle morphogenesis | $1.69 \times 10^{-4}$ | Outflow tract morphogenesis | 0.003296 |
| Heart development | 0.001063 | Cellular response to BMP stimulus | 0.007381 |
| Cardiac muscle cell differentiation | 0.001585 | Primitive streak formation | 0.007493 |
| Secondary heart field specification | 0.002004 | Organ morphogenesis | 0.007911 |
| Outflow tract morphogenesis | 0.007299 | Heart development | 0.037001 |
| Embryonic heart tube development | 0.007223 | BMP signalling pathway involved in heart induction | 0.039664 |

**FIGURE 6** Single-cell (sc) RNA-sequencing (seq) analysis revealed the major affected populations of cardiac mesoderm progenitors in the inhibitors of DNA-binding proteins (IDs) knockout (KO) line. a) Schematic of the differentiation of cardiomyocytes (CMs) differentiated from human embryonic stem cells (hESCs). The mRNA levels of *EOMES*, *MESP1* and *ID1* at different stages were measured by quantitative PCR and revealed that day 4 was the key point during differentiation. b) t-Distributed stochastic neighbour embedding with the R-Seurat package showing the different sources of cells analysed (right) and six clusters for wild-type (WT) and IDs KO lines (left) on day 4 of CM differentiation. c) The z-score-scaled average expression levels of differentially expressed genes for six clusters are shown as a heatmap (top), with the selected lineage-specific markers shown on the right. Representative Gene Ontology (GO) terms of biological processes are shown at the bottom. d) The expression level distributions of

representative marker genes are shown as violin plots across clusters. Cell lines and clusters are represented by different colours. BMP: bone morphogenetic protein.

cells into cardiomyocytes. Using the differentiation protocol employed earlier, the population of cells positive for cTnT and α-Actinin (a marker of mature cardiomyocytes) was completely lost in the three IDs KO lines (figure 5b and figure 5c). Immunoblotting demonstrated that the protein levels of EOMES were reduced in the IDs KO lines compared to the wild-type cell lines (figure 5d). Further characterisation of mesoderm markers showed that the expression levels of *Brachyury*, *MIXL1* and *TBX5* were significantly reduced on day 2 of differentiation. On day 4, the expression of *TBX5*, *GATA4* and *ISL1* was further decreased (figure 5e). This finding suggested that the ID double-knockout hESC lines also had impaired cardiac differentiation, similar to *BMPR2* mutant CHD-PAH iPSCs.

### scRNA-seq analysis revealed the major affected populations of cardiac mesoderm progenitors in the IDs KO line

To examine the effect of *ID* knockout on hESCs differentiation towards cardiac lineages, the single-cell transcriptomes of wild-type and IDs KO hESCs were examined after they were induced to differentiate towards cardiomyocytes. We determined the *ID1* expression in wild-type hESCs during differentiation and observed peak mRNA expression on day 4 (figure 6a). At the same time, we observed the expression of cardiac mesoderm progenitor (CMP) markers, including *EOMES* and *MESP1* (figure 6a).

We then prepared single-cell samples for scRNA-seq according to the 10× Genomics general sample preparation method at day 4. After sequencing and data processing, we obtained high-quality transcriptomic data from 8690 single cells (4761 wild-type and 3929 ID KO cells) after stringent segregation and the removal of floating dead cells that detached during differentiation. Subsequently, unsupervised clustering analysis showed six clusters for the collected live cells and differential expression patterns of wild-type and IDs KO (figure 6b). Then, we combined the original sample information and expression levels of well-known markers to determine the cell identity of each cluster and analysed their biological features by performing Gene Ontology analysis of differentially expressed genes (DEGs). We identified six major cell clusters: C0 was the largest cell cluster, mainly containing neural progenitors with high expression of *STMN2*, *SOX11* and *TUBB2B*. C1 cluster cells were mainly undefined and expressed *CITED2* and *FST*. C2 was a cluster of CMPs that expressed the cardiac mesoderm markers *MESP1*, *HAND1* and *FOXC1*. The C3 cluster was composed of cells expressing high levels of *MKI67*, *CDK1* and *PLK1*, which are involved in cell division and proliferation. Some C4 cluster cells expressed the pluripotency marker *POU5F1* and the metal ion responsive genes *MT2A* and *MT1E*. C5 was a group of cells in the transition state from mesendoderm cells to CMPs that highly expressed *SOX17*, *GATA3* and *ISL1* (figure 6c and 6d). C2 and C5 were mainly composed of wild-type cells, whereas C0 and C1 were mainly composed of IDs KO cells. Taken together, these results suggest that ID1 and ID3 drive mesoderm differentiation towards the cardiac lineage and that the knockout of *ID1* and *ID3* contributes to the emergence of neural marker gene-expressing cells.

### USP9X is a downstream effector gene of ID1 and ID3 in CMPs

Next, we used R-Seurat to analyse cells on day 4 of differentiation into cardiomyocytes to identify differentially regulated genes in CMPs. As shown in the clustering analysis, the majority of cells in CMP-related clusters 2 and 5 were wild-type cells, as very few IDs KO cells were included in these clusters (figure 7a). We further demonstrated that cardiogenesis-related markers (*MESP1*, *HAND1*, *EOMES*, *GATA4* and *BMP4*) and right ventricle specific markers (*ISL1*) were widely expressed in cluster 2 or cluster 5, which mainly consisted of wild-type cells (figure 7a). Surprisingly, we found that *USP9X* (ubiquitin-specific protease 9X) was one of the most differentially affected genes in wild-type cells in most clusters (C0, C1, C2, C3 and C5) compared with IDs KO cells (figure 7b). USP9X, the homologue of *Drosophila* fat facets, is a deubiquitinating enzyme. Loss-of-function mutations in *USP9X* were reported in 17 females that had distinct congenital malformations, including heart defects [20]. The expression of *USP9X* was highest in cluster 2 (figure 7c), and DEG analysis showed that the *USP9X* levels were altered more extensively in CMPs than in other clusters after *ID1/ID3* knockout (figure 7d). Thus, the expression levels of *USP9X* and cardiogenesis-related genes are reduced relative to those in wild-type cells.

### Deficient BMPR2/ID signalling downregulates USP9X through E47 during CHD-PAH iPSC differentiation towards cardiomyocytes

To further investigate whether the protein levels of ID1 and ID3 correlate with USP9X expression, we examined the effect of altered ID1/3 expression on USP9X in differentiated cells *via* immunoblot analysis.
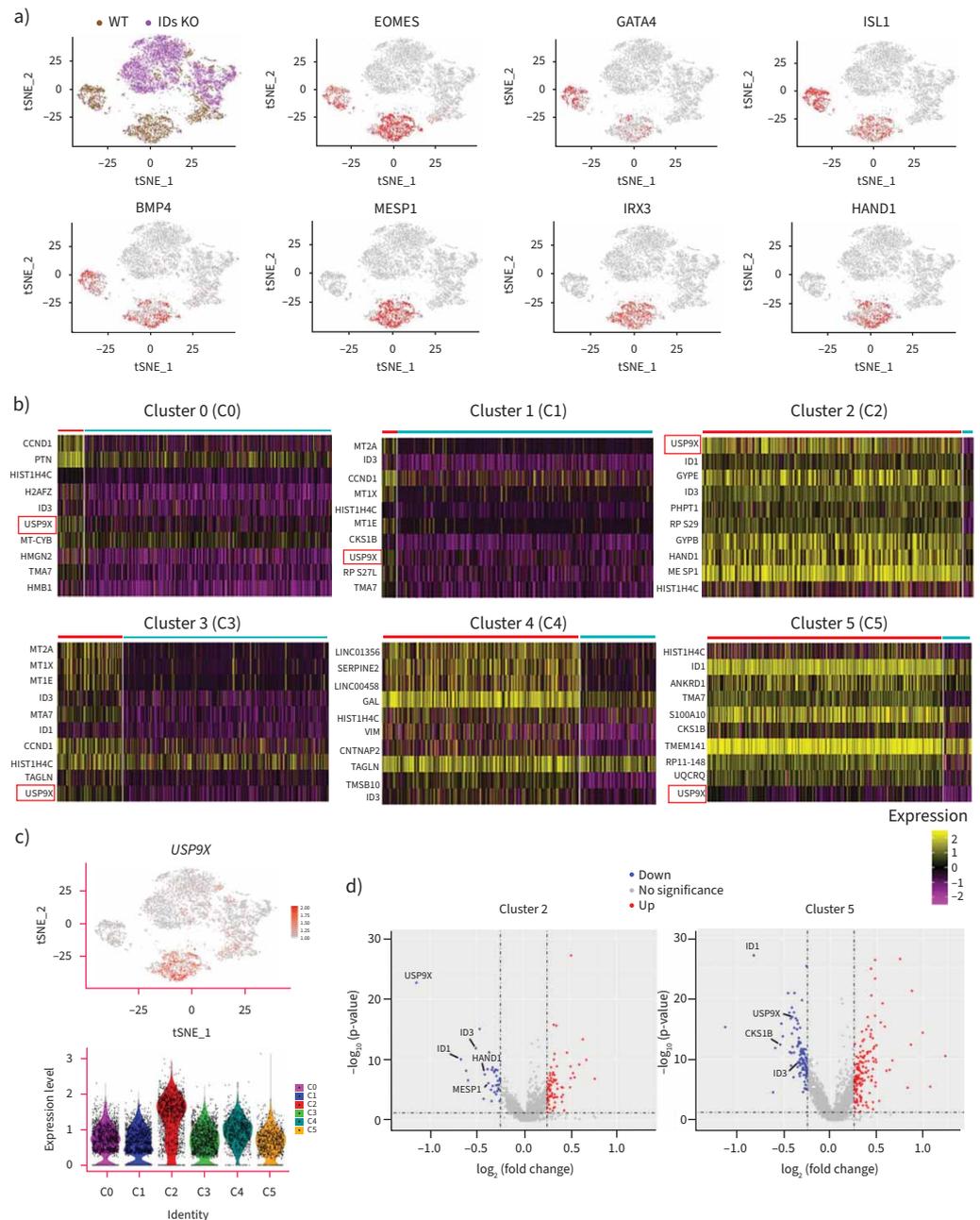
**FIGURE 7** *USP9X* is a downstream effector gene of deficient inhibitors of DNA-binding proteins (IDs) in cardiac mesoderm progenitors (CMPs). a) t-Distributed stochastic neighbour embedding (t-SNE) visualisation of the key marker genes (*EOMES*, *GATA4*, *ISL1*, *BMP4*, *MESP1*, *IRX3* and *HAND1*) in clusters 2 and 5. Cells expressing the representative marker genes are denoted in red. b) The z-score scaled average expression levels of differentially expressed genes (DEGs) between wild-type (WT) cells (red line) and IDs knockout (KO) cells (blue line) for six clusters are shown as heatmaps. c) The expression level distributions of *USP9X* are shown by t-SNE (upper). Cells expressing representative marker genes are denoted in red. The expression level distributions of *USP9X* are shown as violin plots in various clusters (lower). Cell lines and clusters are represented by different colours. d) Differential expression level of *USP9X*, *HAND1* and *MESP1* and other genes are shown in cluster 2 and *USP9X*, *CKS1B* and other genes in cluster 5 as a volcano plot. The size of the dot denotes the percentage of cells within a cluster, while the colour denotes the average expression level across all cells within a cluster.

In the ID KO cells, USP9X expression was lower on day 4 of cardiomyocyte differentiation than in wild-type cells (figure 8a). All three IDs KO lines had obviously reduced USP9X expression compared with that in the three wild-type lines on day 4 (figure 8b). We next examined whether *BMPR2* mutations affected
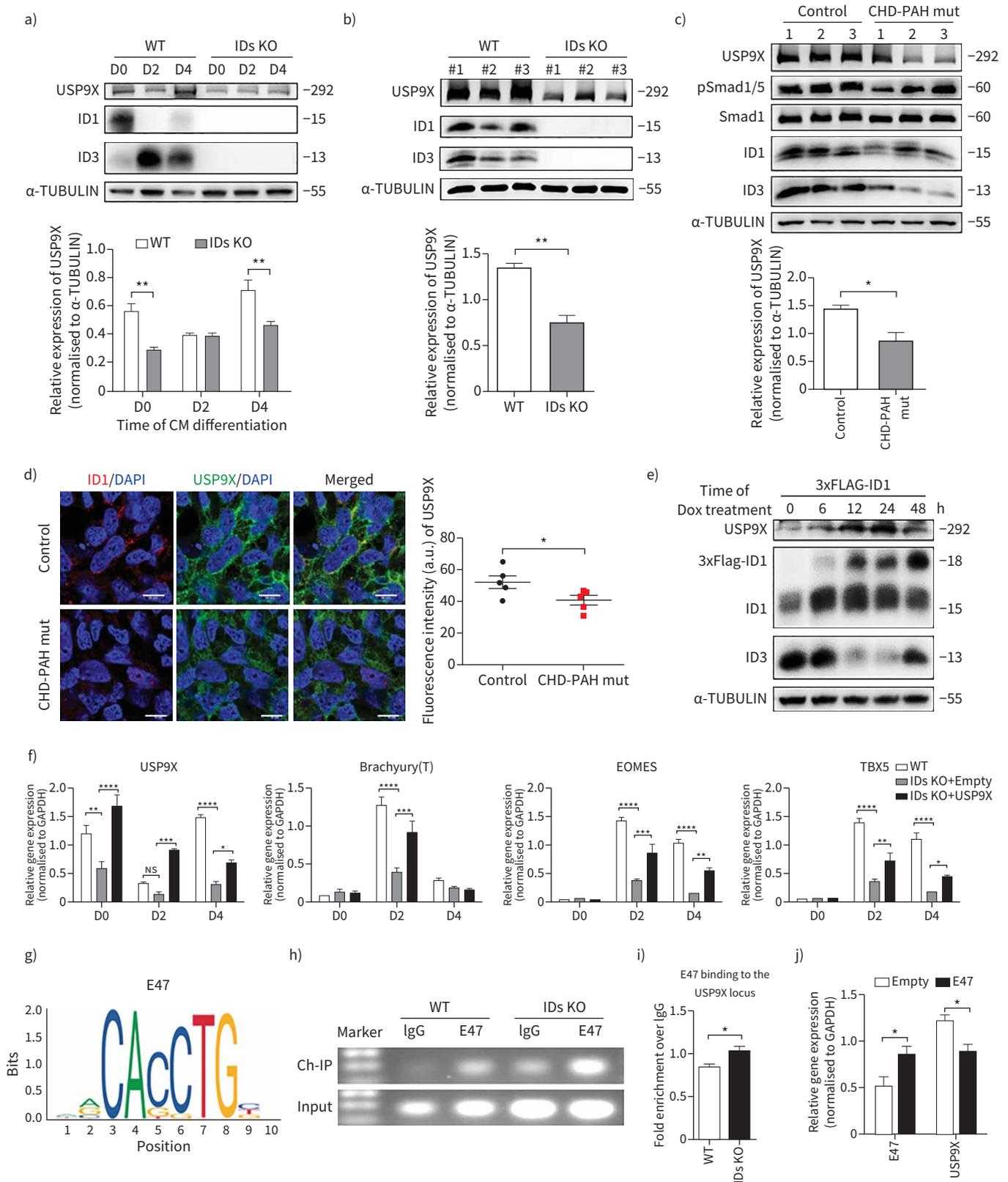
FIGURE 8 Deficient bone morphogenetic protein type II receptor (BMPR2)/inhibitors of DNA-binding protein (ID) signalling downregulates USP9X *via* E47 during cardiomyocyte (CM) differentiation. a, b) Immunoblot analysis and quantification of a) USP9X, ID1 and ID3 in wild-type (WT) and IDs knockout (KO) cells at different stages of CM differentiation and b) in different WT and IDs KO cell lines (three cell lines in each group) on day 4 of CM differentiation. α-TUBULIN was used as the loading control. c) Immunoblot analysis of USP9X, pSmad1/5, ID1 and ID3 expression and

quantification of USP9X in control and congenital heart disease-associated pulmonary arterial hypertension (CHD-PAH) mut induced pluripotent stem cells (iPSCs) on day 4 of CM differentiation. Three cell lines, marked as 1, 2 and 3, were analysed in each group. Total Smad1 and α-TUBULIN were used as loading controls. d) Representative fluorescence intensity of ID1 (red) and USP9X (green) (left) and the corresponding ImageJ-based quantifications (right) of the fluorescence intensity in the cells on day 4 of CM differentiation from control or CHD-PAH mut iPSCs. n=5, five random fields. Scale bars=50 μm. e) Immunoblot analysis of USP9X, ID1 (endogenous (lower band) and exogenous (upper band)) and ID3 expression in h9-ESC-3F-ID1 cells with 3×Flag-ID1 overexpression induced by Dox (2 μg·mL$^{-1}$) at different time points. α-TUBULIN was used as the loading control. f) The mRNA levels in WT, IDs KO+empty (IDs KO overexpressing an empty vector in), and IDs KO+USP9X (overexpressing USP9X in IDs KO) cells on various days during CM differentiation as measured by quantitative (q)PCR. n=3, three technical replicates for one cell line. g) Predicted DNA binding site motif of E47 in the *USP9X* promoter region. h, i) The *USP9X* promoter region in WT and IDs KO cells pulled down with an E47 antibody was detected by chromatin immunoprecipitation (ChIP)-PCR h) and ChIP-qPCR i). n=3 in panel i). j) The mRNA levels in WT cells after transfection with E47 or empty vector as determined by qPCR. n=3. All results are presented as mean±SEM. *: p<0.05, **: p<0.01, ***: p<0.001, ****: p<0.0001 were determined using two-way ANOVA with *post hoc* tests (Sidak's multiple comparisons test) (a and j), two-way ANOVA with *post hoc* tests (Tukey's multiple comparisons test) (f) or unpaired t-tests (b–d and i).

the cardiomyocyte differentiation in CHD-PAH iPSCs *via* USP9X. We differentiated CHD-PAH iPSCs with *BMPR2* mutations into beating cardiomyocytes and examined downstream signalling. On day 4, Smad1/5 phosphorylation as well as ID1, ID3 and USP9X expression was reduced in these CHD-PAH cells compared to control cells (figure 8c). Immunofluorescence staining also showed reduced USP9X expression in the cytoplasm of CHD-PAH mut differentiated cells (figure 8d). In addition, we overexpressed ID1 to confirm the correlation and found that USP9X expression was increased following the induction of ID1 protein expression, and a corresponding reduction in ID3 expression was observed (figure 8e). During cardiomyocyte differentiation, the levels of *EOMES* and *TBX5* were significantly reduced in in IDs KO cells compared with wild-type cells (figure 5e and figure 8f). Overexpression of USP9X in IDs KO cells enhanced the expression of *EOMES* and *TBX5* on days 2 and 4 of cardiomyocyte differentiation compared to that in IDs KO+empty cells (figure 8f). Therefore, the reduction of cardiogenesis-related marker expression caused by *ID1* and *ID3* knockout were rescued by USP9X overexpression.

To study the regulatory effects of IDs on downstream gene expression, we examined possible ID binding partners, such as E47, an E protein transcription factor that contains a basic DNA-binding region juxtaposed to an HLH domain. Without the DNA-binding region, ID proteins have only an HLH domain with which to form heterodimers with E47 and thereby compete for binding with other E proteins to inhibit the transcription of target genes. Based on a previous report that E47 represses cariogenic mesoderm gene expression [12], we further found that the *USP9X* promoter region contains the E47 binding site sequence (CACCTG) by searching JASPAR (http://jaspar.genereg.net) (figure 8g). A chromatin immunoprecipitation-PCR assay revealed that the binding of E47 to the *USP9X* promoter was increased in IDs KO cells (figure 8h and figure 8i). Furthermore, we overexpressed E47 and observed reduced *USP9X* levels as determined by quantitative PCR (figure 8j), indicating the inhibitory effect of E47 on *USP9X* gene transcription. Our results suggest that mutant *BMPR2* signals *via* ID1, leading to the accumulation of E47 on the *USP9X* promoter, which negatively regulates *USP9X* gene expression during cardiomyocyte differentiation (figure 9).

## Discussion

Although pulmonary load is thought to be important for right ventricular function in patients with PAH, there are some genetic determinants for right ventricular failure. We are interested in the impact of individual components of the BMPR2 signalling pathway on mesoderm formation during gastrulation [12, 21]. Determining whether IDs contribute to right heart failure in PAH patients carrying *BMPR2* mutations continues to be challenging. Our results showed that in iPSC-cardiomyocytes from CHD-PAH patients with BMP receptor mutations, the total ID protein level was reduced, and the cardiomyocyte differentiation efficiency and Ca$^{2+}$ handling were affected. We detected reduced Ca$^{2+}$ transients, τ decay and half decay time, but the half rising time and time to peak were not altered in mutant iPSC-cardiomyocytes. In addition, we confirmed reduced ID1/ID3 expression in the right heart samples from *Bmpr2$^{+/-}$* rats. By generating conditional knockouts, we circumvented the embryonic lethality in double KO Id1/3 mice and found that some Ids cDKO mice spontaneously developed PAH. SPAH was defined by a mean pulmonary arterial pressure (mPAP) ⩾25 mmHg by HAUTEFORT *et al.* [8]. Their *Bmpr2*-deficient rats developed SPAH in an age-dependent manner, with the incidence rate ranging between 16.7% and 27.8%, perfectly mimicking the PAH incidence in patients with *BMPR2* mutations. Additionally, susceptibility to SPAH was concurrent with the high levels of perivascular fibrillar collagen. In figure 3 we demonstrated pulmonary vascular remodelling in the SPAH group, whereas no obvious difference at remodelling rate of pulmonary arteries in "nonspontaneous PAH" compared with control mice was detected. We found that a
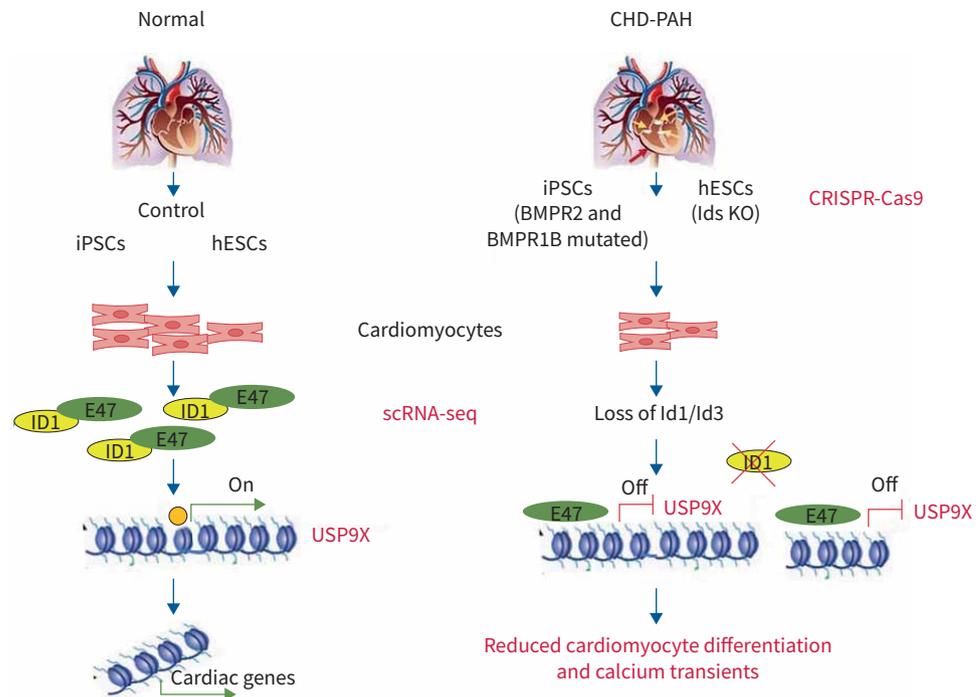
**FIGURE 9** By using bone morphogenetic protein (BMP) receptor mutant congenital heart disease-associated pulmonary arterial hypertension (CHD-PAH) patient induced pluripotent stem cells (iPSCs) together with single-cell RNA sequencing (scRNA-seq) on inhibitors of DNA-binding proteins (IDs) knockout (KO) human embryonic stem cells (hESCs), we found that BMPR2 signals *via* IDs and USP9X to drive cardiac differentiation. In normal controls, BMPR2 signals *via* ID1, leading to the inhibition of E47 binding on the *USP9X* promoter, which regulates *USP9X* gene expression during cardiomyocyte differentiation. In CHD-PAH patients with BMP receptor mutations, the loss of ID1 and ID3 expression contributes to CM dysfunction.

few Ids cDKO mice had ventricular defects or pulmonary regurgitation. The reduced $Ca^{2+}$ transients and sarcomere length shortening could be responsible for the reduction in cardiac output in Ids cDKO mice, which was consistent with the compromised cardiomyocyte function in *Bmpr2$^{+/-}$*rats. However, many factors have not been clarified, such as the downstream tissue-specific targets of *IDs*.

To further study the heart-specific effects of ID1/3, we employed scRNA-seq analysis, which can advantageously classify mixed cells according to their gene expression and identify new cell types or marker genes [22]. In our study, the scRNA-seq results clearly demonstrated that the cardiomyocyte differentiation of IDs KO cells was impaired and that clusters 2 and 5, which expressed CMP related genes, were the major populations affected in IDs KO cells. DEG analysis revealed that USP9X expression was reduced in most clusters of IDs KO cells compared with the wild-type cell clusters. We also showed a reduction in USP9X expression during the cardiomyocyte differentiation of CHD-PAH patient-derived iPSCs. These findings advance the current understanding of the specific effects of *BMPR2* mutations on the heart.

It is worth mentioning that hESCs and hiPSCs share the same characteristics, including their expression of pluripotent markers and their differentiation potential. How *BMPR* mutations affect heart development should be investigated in the early stage of hESC differentiation when BMPs act *via* receptors to drive cardiac mesoderm formation. In hESC culture medium, Essential 6 medium (E6) does not contain fibroblast growth factor or transforming growth factor-β, which are included in Essential 8 medium (E8). E6 does not maintain pluripotency in hESCs because of the lack of these two growth factors, which reduced the level of Smad1 phosphorylation. To reduce basal activation of smad1, signal transduction was assessed mainly in E8, with which we found ID1 and ID3 were coordinately regulated downstream of BMPR2 in hESCs (figure 2).

This study has several limitations. First, IDs are not exclusively regulated by BMPR2. Different mutations in BMPR2 signalling pathway components (which cause PAH), such as those of *BMPR1B* (CHD-PAH 4), also downregulate ID expression (supplementary table S1, supplementary figure S3). Other mutations in

BMPR2 signalling components also converge at IDs to potentiate PAH [23], and vascular endothelial growth factor (VEGF) can induce ID expression [24]. We consistently observed reduced ID1 expression in Sugen 5416 (VEGF inhibitor)/hypoxia PAH rats [25]. Although knocking-out a single factor *IDs* recapitulated heart defects in BMPR2$^{flox/-}$;Mox2-cre mice, comparable *BMPR2* cardiomyocyte-specific knockout animals have not been studied in the PAH setting. Second, the *Bmpr2*$^{+/-}$ heterozygous rats had some phenotypic differences, such as differential RVSPs, which could be explained mainly by differences in the rat strains since the two groups targeted *BMPR2* to generate a frame shift in exon 1 [26]. It is worth examining aborted embryos to identify possible heart defects.

*BMPR2* mutations occur among three shunt types (VSD, ASD and PDA) at similar frequencies in CHD-PAH patients [4]. For example, CHD-PAH mut 2 (AZ2) provided a rationale for determining the presence or absence of a *BMPR* mutation in a patient with CHD-PAH. The patient had a PDA defect with mPAP 79 mmHg, PVR of 19.5 Wood Units (>5 WU), and a pulmonary to systemic flow ratio of 0.85 (<1.5), which was not within the surgical closure indication. He developed much more severe PAH than that caused by a PDA defect. Another female ASD patient with CHD-PAH mut 3 (AZ3) developed severe PAH at a younger age than most patients (mPAP 31 mmHg, PVR 9.38 WU). She was shown to carry the c.1042G>A mutation in *BMPR2* exon 8, which prompted predictive genetic testing in unaffected relatives. We found that her father and sister had the same mutation despite having no symptoms thus far (supplementary table S9).

Among the *BMPR2* mutations we detected in CHD-PAH patients, nearly all were missense mutations [4]. Five types of *BMPR2* mutations exist for H/IPAH: nonsense, deletion, frameshift, splice site and missense. The relationships between the phenotypes and mutation types are worthy of further exploration. The patients with CHD-PAH had much more severe clinical manifestations than those normally caused by the defects should undergo genetic testing to detect abnormalities of BMPR2 and its downstream components. Mutation carriers are more at risk for PAH reoccurrence than those without *BMPR2* mutations and should be monitored even after surgical closure of the shunt. From our study it was recommended to include USP9X and BMPR2 signalling components in the risk gene panel to screen CHD-PAH patients who have out-of-proportion PAH in relation to a (small) shunt (small ASD or VSD) or sustained/progressive PAH after shunt closure with PAH in the setting of cardiovascular left-to-right shunt. Targeted therapies or transplantation could be considered for these patients in the early stage of the disease.

### Conclusion

By using a number of methods, including iPSC generation and differentiation, scRNA sequencing of CRISPR/CAS9-targeted hESCs and Ids cDKO mouse cardiomyocyte functional assays, we found that BMPR2 signals *via* IDs and USP9X to drive cardiac differentiation. The loss of ID1 and ID3 expression contributes to cardiomyocyte dysfunction in CHD-PAH patients with *BMPR2* mutations.

## References

1 Runo JR, Loyd JE. Primary pulmonary hypertension. *Lancet* 2003; 361: 1533–1544.

2 Zaiman A, Fijalkowska I, Hassoun PM, *et al.* One hundred years of research in the pathogenesis of pulmonary hypertension. *Am J Respir Cell Mol Biol* 2005; 33: 425–431.

3 Roberts KE, McElroy JJ, Wong WP, *et al.* BMPR2 mutations in pulmonary arterial hypertension with congenital heart disease. *Eur Respir J* 2004; 24: 371–374.

4 Liu D, Liu QQ, Guan LH, *et al.* BMPR2 mutation is a potential predisposing genetic risk factor for congenital heart disease associated pulmonary vascular disease. *Int J Cardiol* 2016; 211: 132–136.

5 Morrell NW, Yang X, Upton PD, *et al.* Altered growth responses of pulmonary artery smooth muscle cells from patients with primary pulmonary hypertension to transforming growth factor-$\beta_1$ and bone morphogenetic proteins. *Circulation* 2001; 104: 790–795.

6 Long L, Ormiston ML, Yang X, *et al.* Selective enhancement of endothelial BMPR-II with BMP9 reverses pulmonary arterial hypertension. *Nat Med* 2015; 21: 777–785.

7 Beppu H, Malhotra R, Beppu Y, *et al.* BMP type II receptor regulates positioning of outflow tract and remodeling of atrioventricular cushion during cardiogenesis. *Dev Biol* 2009; 331: 167–175.

8 Hautefort A, Mendes-Ferreira P, Sabourin J, *et al.* Bmpr2 mutant rats develop pulmonary and cardiac characteristics of pulmonary arterial hypertension. *Circulation* 2019; 139: 932–948.

9 Zhao QS, Beck AJ, Vitale JM, *et al.* Developmental ablation of Id1 and Id3 genes in the vasculature leads to postnatal cardiac phenotypes. *Dev Biol* 2011; 349: 53–64.

10 Fraidenraich D, Stillwell E, Romero E, *et al.* Rescue of cardiac defects in id knockout embryos by injection of embryonic stem cells. *Science* 2004; 306: 247–252.

11 Yang J, Li X, Morrell NW. Id proteins in the vasculature: from molecular biology to cardiopulmonary medicine. *Cardiovasc Res* 2014; 104: 388–398.

12 Cunningham TJ, Yu MS, McKeithan WL, *et al.* Id genes are essential for early heart formation. *Genes Dev* 2017; 31: 1325–1338.

13 Chou BK, Mali P, Huang X, *et al.* Efficient human iPS cell derivation by a non-integrating plasmid from blood cells with unique epigenetic and gene expression signatures. *Cell Res* 2011; 21: 518–529.

14 Xie Y, Wang D, Lan F, *et al.* An episomal vector-based CRISPR/Cas9 system for highly efficient gene knockout in human pluripotent stem cells. *Sci Rep* 2017; 7: 2320.

15 Astorga J, Carlsson P. Hedgehog induction of murine vasculogenesis is mediated by Foxf1 and Bmp4. *Development* 2007; 134: 3753–3761.

16 Jiao K, Kulessa H, Tompkins K, *et al.* An essential role of Bmp4 in the atrioventricular septation of the mouse heart. *Genes Dev* 2003; 17: 2362–2367.

17 Hollnagel A, Oehlmann V, Heymer J, *et al.* Id genes are direct targets of bone morphogenetic protein induction in embryonic stem cells. *J Biol Chem* 1999; 274: 19838–19845.

18 Ying QL, Nichols J, Chambers I, *et al.* BMP induction of Id proteins suppresses differentiation and sustains embryonic stem cell self-renewal in collaboration with STAT3. *Cell* 2003; 115: 281–292.

19 Yamasaki A, Kasai A, Toi A, *et al.* Identification of the role of bone morphogenetic protein (BMP) and transforming growth factor-β (TGF-β) signaling in the trajectory of serotonergic differentiation in a rapid assay in mouse embryonic stem cells *in vitro*. *J Neurochem* 2015; 132: 418–428.

20 Reijnders MR, Zachariadis V, Latour B, *et al.* De novo loss-of-function mutations in USP9X cause a female-specific recognizable syndrome with developmental delay and congenital malformations. *Am J Hum Genet* 2016; 98: 373–381.

21 Bernardo AS, Faial T, Gardner L, *et al.* BRACHYURY and CDX2 mediate BMP-induced differentiation of human and mouse pluripotent stem cells into embryonic and extraembryonic lineages. *Cell Stem Cell* 2011; 9: 144–155.

22 Scialdone A, Tanaka Y, Jawaid W, *et al.* Resolving early mesoderm diversification through single-cell expression profiling. *Nature* 2016; 535: 289–293.

23 Hodgson J, Swietlik EM, Salmon R, *et al.* Characterization of *GDF2* mutations and levels of BMP9 and BMP10 in pulmonary arterial hypertension. *Am J Respir Crit Care Med* 2020; 201: 575–585.

24 Sakurai D, Tsuchiya N, Yamaguchi A, *et al.* Crucial role of inhibitor of DNA binding/differentiation in the vascular endothelial growth factor-induced activation and angiogenic processes of human endothelial cells. *J Immunol* 2004; 173: 5801–5809.

25    Xing Y, Zhao S, Wei Q, *et al.* A novel piperidine identified by stem cell-based screening attenuates pulmonary arterial hypertension by regulating BMP2 and PTGS2 levels. *Eur Respir J* 2018; 51: 1702229.

26    Tian W, Jiang X, Sung YK, *et al.* Phenotypically silent bone morphogenetic protein receptor 2 mutations predispose rats to inflammation-induced pulmonary arterial hypertension by enhancing the risk for neointimal transformation. *Circulation* 2019; 140: 1409–1425.